Title

Two-dimensional axisymmetric formulation of high order spherical harmonics methods for radiative heat transfer

Authors

Ge, Wenjun
Modest, Michael F
Marquez, Ricardo

Publication Date

2015-05-01

DOI

10.1016/j.jqsrt.2015.01.013

Peer reviewed

Journal of Quantitative Spectroscopy & Radiative Transfer 156 (2015) 58–66

Contents lists available at ScienceDirect

Journal of Quantitative Spectroscopy & Radiative Transfer

journal homepage: www.elsevier.com/locate/jqsrt

Two-dimensional axisymmetric formulation of high order spherical harmonics methods for radiative heat transfer

Wenjun Ge, Michael F. Modest*, Ricardo Marquez

University of California, Merced 95343, United States

ARTICLE INFO

Article history:
Received 15 September 2014
Received in revised form
7 January 2015
Accepted 24 January 2015
Available online 7 February 2015

Keywords:
Radiative transfer
RTE solver
Spherical harmonics
High order spherical harmonics
P_N-approximation
Axisymmetric

ABSTRACT

The spherical harmonics (P_N) method is a radiative transfer equation solver, which approximates the radiative intensity as a truncated series of spherical harmonics. For general 3-D configurations, $N(N+1)/2$ intensity coefficients must be solved from a system of coupled second-order elliptic PDEs. In 2-D axisymmetric applications, the number of equations and intensity coefficients reduces to $(N+1)^2/4$ if the geometric relations of the intensity coefficients are taken into account. This paper presents the mathematical details for the transformation and its implementation on the *OpenFOAM* finite volume based CFD software platform. The transformation and implementation are applicable to any arbitrary axisymmetric geometry, but the examples to test the new formulation are based on a wedge grid, which is the most common axisymmetric geometry in CFD simulations, because *OpenFOAM* and most other platforms do not have true axisymmetric solvers. Two example problems for the new axisymmetric P_N formulation are presented, and the results are verified with that of the general 3-D P_N solver, a Photon Monte Carlo solver and exact solutions.

1. Introduction

The study of radiative heat transfer in high-temperature applications with a strongly varying participating medium has become increasingly important in various practical applications like combustion, manufacturing and environmental systems. The Radiative Transfer Equation (RTE) is an integro-differential equation in six independent variables (3 spatial and 2 directional, and wavenumber) [1], which is exceedingly difficult to solve. As a result, approximate solution methods to the RTE, such as the spherical harmonics method (SHM), discrete ordinates method (DOM), the finite volume method (FVM), or the Monte Carlo method are frequently employed to solve radiation problems. Each of these approximate methods has their well-known advantages and drawbacks. The SHM offers an approximate solution to the radiative transfer equation (RTE) by transforming the RTE into a system of elliptic PDEs. This method approximates the radiative intensity as a truncated series of spherical harmonics that decouple the directional and spatial variations of the intensity field. The SHM has been widely applied to particle transport problems [2–4], and some of the derivations for cylindrical geometries have been presented in [5,6].

For axisymmetric problems, physical quantities such as temperature, heat flux, radiative intensity, and chemical species concentrations vary only radially and axially and are, therefore, two-dimensional. As a result, for many of these applications, the transport equations are solved on a 2-D or a thin wedge 3-D computational domain in order to reduce the computational effort. Like the development of the general P_N method [7,8], the application of axisymmetric formulations of P_N method were limited [9,10]

* Corresponding author.
E-mail address: mmodest@ucmerced.edu (M.F. Modest).

http://dx.doi.org/10.1016/j.jqsrt.2015.01.013
0022-4073/

because of the cumbersome mathematics. Recently, the general P_N (up to P_7) equations and boundary conditions for 3-D geometries have been formulated [11–13] and solved [14] for various cases including a full cylinder with variable radiative properties and a real flame.

In this paper, the 2-D axisymmetric version of P_N and its boundary conditions are deduced from the 3-D P_N formulation. The 2-D axisymmetric formulation is implemented in *OpenFOAM* [15] C++ open source libraries. *OpenFOAM* provides the mesh generator, the numerical PDE solvers and the input/output handlers for the example problems shown in this paper. It also includes various CFD calculation modules, which the radiation module can be directly coupled with. Like other modern CFD codes, *OpenFOAM* uses the finite-volume method with unstructured mesh topology. A wedge is the most common way to represent an axisymmetric full cylinder in the finite-volume CFD simulation. Thus, the 2-D axisymmetric example cases in this paper are based on a 3-D finite-volume wedge. Demonstration problems presented here are the 3-D wedge versions of axisymmetric cases presented in [14]. The results of high-order P_N are found to be very close to the exact solution of the RTE, and the results are also verified against those of the 3-D P_N solver.

2. Formulation

***Axisymmetric conditions*:** The radiative transfer equation (RTE) is an integro-differential equation with spatial and directional dependence [1],

$$\hat{s}\cdot\nabla_{\boldsymbol{\tau}} I + I = (1-\omega)I_b + \frac{\omega}{4\pi}\int_{4\pi} I(\hat{s}')\Phi(\hat{s}\cdot\hat{s}')\,d\Omega' \tag{1}$$

where $\boldsymbol{\tau} = \int \beta_r\, d\mathbf{r}$ is an optical coordinate, and β_r is the radiative extinction coefficient; I_b is the blackbody radiative intensity (Planck function); and ω is the scattering albedo. The P_N approximation is based on approximating the radiative intensity field $I(\boldsymbol{\tau},\hat{\mathbf{s}})$ as a series of products of intensity coefficients I_n^m and spherical harmonics Y_n^m, whereby the spatial and the directional ($\hat{\mathbf{s}}$) dependencies are decoupled:

$$I(\boldsymbol{\tau},\hat{\mathbf{s}}) = \sum_{n=0}^{N}\sum_{m=-n}^{n} I_n^m(\boldsymbol{\tau})Y_n^m(\hat{\mathbf{s}}) \tag{2}$$

Spherical harmonics satisfy Laplace's equation in spherical coordinates and are defined here as

$$Y_n^m = \begin{cases} \cos(m\psi)P_n^m(\cos\theta) & \text{for } m \geq 0 \\ \sin(|m|\psi)P_n^m(\cos\theta) & \text{for } m < 0 \end{cases} \tag{3}$$

and $P_n^m(\cos\theta)$ are associated Legendre polynomials. The position-dependent intensity coefficients $I_n^m(\boldsymbol{\tau})$ are determined by applying the series approximation to the RTE.

The radiative intensity depends on position $\mathbf{r}(r,\phi,z)$ and direction $\hat{\mathbf{s}}(\theta,\psi)$ where θ is the polar angle (measured from the z-axis), and ψ is the azimuthal angle (measured counter-clockwise from the x-axis). If the physical system is axisymmetric, then the radiative intensity varies radially with r and axially with z, but not azimuthally with ϕ. Fig. 1 illustrates several location–direction combinations, which have identical intensities for axisymmetric conditions. At a

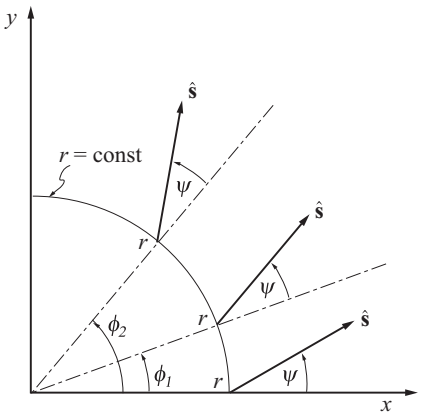

Fig. 1. Illustration of the invariance of intensity with respect to azimuthal angle ψ at different locations for axisymmetric conditions.

fixed location $\mathbf{r}(r,\phi_1,z)$ the radiative intensity in the direction $\hat{\mathbf{s}}(\theta,\psi+\phi_1)$ is equal to the radiative intensity at some other location $\mathbf{r}(r,\phi_2,z)$ in the direction $\hat{\mathbf{s}}(\theta,\psi+\phi_2)$, which has the same deflection angle relative to its position vector $\mathbf{r}$. One may conclude from Fig. 1 that

$$I(r,\phi,z;\theta,\psi+\phi) = I(r,0,z;\theta,\psi) \tag{4}$$

for any ϕ, as long as the problem is axisymmetric. When $\phi=0$, the radiative intensity is evaluated along the x-axis. Considering the general case at some arbitrary ϕ and a reference case when $\phi=0$, the radiative intensity as approximated by the spherical harmonic series expansion equation (2) yields, for a given n, the equality

$$\begin{aligned} &I_n^0(r,\phi,z)P_n^0(\theta) + \sum_{m=1}^{n} I_n^m(r,\phi,z)[\cos m\psi\cos m\phi \\ &\quad - \sin m\psi\sin m\phi]P_n^m(\theta) \\ &\quad + \sum_{m=1}^{n} I_n^{-m}(r,\phi,z)[\sin m\psi\cos m\phi + \cos m\psi\sin m\phi]P_n^m(\theta) \\ &= I_n^0(r,0,z)P_n^0(\theta) + \sum_{m=1}^{n} I_n^m(r,0,z)\cos m\psi P_n^m(\theta) \\ &\quad + \sum_{m=1}^{n} I_n^{-m}(r,0,z)\sin m\psi P_n^m(\theta) \end{aligned} \tag{5}$$

By comparing the I_n^0 terms, it follows that for $m=0$

$$I_n^0(r,\phi,z) = I_n^0(r,0,z) \tag{6}$$

which implies that the intensity coefficients with $m=0$ must be functions of r and z only and are thus axisymmetric. Now comparing other like terms, $\cos m\psi P_n^m(\cos\theta)$ and $\sin m\psi P_n^m(\cos\theta)$ in Eq. (5), yields the following relations for intensity coefficients with $m>0$:

$$I_n^m(r,0,z) = I_n^m(r,\phi,z)\cos m\phi + I_n^{-m}(r,\phi,z)\sin m\phi \tag{7a}$$

$$I_n^{-m}(r,0,z) = -I_n^m(r,\phi,z)\sin m\phi + I_n^{-m}(r,\phi,z)\cos m\phi \tag{7b}$$

Inverting these relations to express $I_n^m(r,\phi,z)$ and $I_n^{-m}(r,\phi,z)$ in terms of the $I_n^m(r,0,z)$ and $I_n^{-m}(r,0,z)$ gives

$$I_n^m(r,\phi,z) = I_n^m(r,0,z)\cos m\phi - I_n^{-m}(r,0,z)\sin m\phi \tag{8a}$$

$$I_n^{-m}(r,\phi,z) = I_n^m(r,0,z)\sin m\phi + I_n^{-m}(r,0,z)\cos m\phi \tag{8b}$$

Also, by symmetry at $\phi=0$, $I(r,0,z;\theta,\psi)=I(r,0,z;\theta,-\psi)$, or

$$\sum_{m=1}^{n} I_n^m(r,0,z)Y_n^m(\psi,\theta)=\sum_{m=1}^{n} I_n^m(r,0,z)Y_n^m(-\psi,\theta) \tag{9}$$

which leads to $I_n^{-m}(r,0,z)=0$ for any m. Thus, according to Eqs. (8), the intensity coefficients for arbitrary ϕ are related to the same r and z-dependent variable $I_n^m(r,0,z)$ as

$$I_n^m(r,\phi,z)=I_n^m(r,0,z)\cos m\phi \tag{10a}$$

$$I_n^{-m}(r,\phi,z)=I_n^m(r,0,z)\sin m\phi \tag{10b}$$

For axisymmetric problems, the dependence on ϕ of intensity coefficients with $m>0$ are trigonometric factors (sines and cosines with periodicity equal to m) that multiply the same axisymmetric variable $I_n^m(r,0,z)$. Hereafter, this axisymmetric variable will be denoted as $\hat{I}_n^m(r,z)$. From Eqs. (10), it can be seen that the number of intensity coefficient variables of the P_N-approximation is reduced from $N(N+1)/2$ to $(N+1)^2/4$.

Governing equations: As formulated in [11] and simplified for isotropic scattering in [13], a set of $N(N+1)/2$ second-order elliptic PDEs result after applying Eq. (2) to the RTE, with the same number of dependent variables I_n^m. Each PDE is associated with a spherical harmonic Y_n^m and the differential operators are originally in Cartesian coordinates. To obtain the transformation of the PDEs for cylindrical coordinates, the relations of the differential operators are employed:

$$\mathcal{L}_x=\frac{1}{\beta_r}\frac{\partial}{\partial x}=\frac{\cos\phi}{\beta_r}\frac{\partial}{\partial r}-\frac{\sin\phi}{\beta_r r}\frac{\partial}{\partial\phi} \tag{11a}$$

$$\mathcal{L}_y=\frac{1}{\beta_r}\frac{\partial}{\partial y}=\frac{\sin\phi}{\beta_r}\frac{\partial}{\partial r}+\frac{\cos\phi}{\beta_r r}\frac{\partial}{\partial\phi} \tag{11b}$$

$$\mathcal{L}_z=\frac{1}{\beta_r}\frac{\partial}{\partial z} \tag{11c}$$

Together with the coordinates transformation, the $(N+1)^2/4$ governing equations of the 2-D, axisymmetric formulation of the P_N-approximation can be derived from the general 3-D P_N governing equations with the axisymmetric relations of the intensity coefficients. Substituting Eqs. (10) for the $I_n^{\pm m}$ of the 3-D P_N governing equations, after considerable algebra, leads to a transformed set of PDEs for axisymmetric variables $\hat{I}_n^m$ as:

For each Y_n^m: $n=0,2,4,\ldots,(N-1)$ and $m=0,1,2,\ldots,n$:

$$\begin{aligned}
\sum_{k=1}^{3}\Bigg\{&(1+\delta_{m2})a_k^{nm}\cos m\phi\left[\mathcal{L}_{rr}-\frac{2m-3}{\beta_r r}\mathcal{L}_r\right.\\
&\left.+\frac{m(m-2)}{\beta_r^2 r^2}-\frac{m-2}{r}\mathcal{L}_r\left(\frac{1}{\beta_r}\right)\right]\hat{I}_{n+4-2k}^{m-2}\\
&+(1+\delta_{m1})b_k^{nm}\cos m\phi\left[\mathcal{L}_{rz}+\mathcal{L}_{zr}-\frac{2(m-1)}{\beta_r r}\mathcal{L}_z\right.\\
&\left.-\frac{m-1}{r}\mathcal{L}_z\left(\frac{1}{\beta_r}\right)\right]\hat{I}_{n+4-2k}^{m-1}\\
&+\frac{\delta_{m1}}{2}c_k^{nm}\cos\phi\left[\mathcal{L}_{rr}+\frac{1}{\beta_r r}\mathcal{L}_r-\frac{1}{r^2\beta_r^2}+\frac{1}{r}\mathcal{L}_r\left(\frac{1}{\beta_r}\right)\right]\hat{I}_{n+4-2k}^{m}\\
&+d_k^{nm}\cos m\phi\left[\mathcal{L}_{rz}+\mathcal{L}_{zr}+\frac{2(m+1)}{\beta_r r}\mathcal{L}_z+\frac{m+1}{r}\mathcal{L}_z\left(\frac{1}{\beta_r}\right)\right]\hat{I}_{n+4-2k}^{m+1}\\
&+e_k^{nm}\cos m\phi\left[\mathcal{L}_{rr}+\frac{2m+3}{\beta_r r}\mathcal{L}_r+\frac{m(m+2)}{\beta_r^2 r^2}+\frac{m+2}{r}\mathcal{L}_r\left(\frac{1}{\beta_r}\right)\right]\hat{I}_{n+4-2k}^{m+2}\\
&+c_k^{nm}\cos m\phi\left(\mathcal{L}_{rr}+\frac{1}{\beta_r r}\mathcal{L}_r-\frac{m^2}{\beta_r^2 r^2}-2\mathcal{L}_{zz}\right)\hat{I}_{n+4-2k}^{m}\Bigg\}\\
&+\cos m\phi\left[\mathcal{L}_{zz}-(1-\omega\delta_{0n})\right]\hat{I}_n^m=-(1-\omega)I_b\delta_{0n}
\end{aligned} \tag{12}$$

where $a_k^{nm}, b_k^{nm}, c_k^{nm}, d_k^{nm}$, and e_k^{nm} are constant coefficients given in [1,13], and δ_{ij} is the Kronecker delta function. The differential operators in cylindrical coordinates are defined as

$$\mathcal{L}_r=\frac{1}{\beta_r}\frac{\partial}{\partial r} \tag{13a}$$

$$\mathcal{L}_{rr}=\frac{1}{\beta_r}\frac{\partial}{\partial r}\left(\frac{1}{\beta_r}\frac{\partial}{\partial r}\right) \tag{13b}$$

$$\mathcal{L}_{rz}=\frac{1}{\beta_r}\frac{\partial}{\partial r}\left(\frac{1}{\beta_r}\frac{\partial}{\partial z}\right) \tag{13c}$$

$$\mathcal{L}_{zr}=\frac{1}{\beta_r}\frac{\partial}{\partial z}\left(\frac{1}{\beta_r}\frac{\partial}{\partial r}\right) \tag{13d}$$

and $\mathcal{L}_r(1/\beta_r)$ is a material property calculated from Eq. (13a) as

$$\mathcal{L}_r\left(\frac{1}{\beta_r}\right)=-\frac{1}{\beta_r^3}\frac{\partial\beta_r}{\partial r} \tag{14}$$

It is noted that each term contains $\cos m\phi$, which may, therefore, be canceled (including the case of $m=0$, for which $\cos m\phi=1$). Each Y_n^{-m} $(m=1,2,\ldots,n)$ returns the same equation as the corresponding Y_n^m, but with $\sin m\phi$ in each term instead of the $\cos m\phi$. Thus, the set of governing equations, like the number of unknown $\hat{I}_n^m$, are reduced to:

For each Y_n^m: $n=0,2,\ldots,N+1$ and $m=0,1,2,\ldots,n$:

$$\begin{aligned}
\sum_{k=1}^{3}\Bigg\{&(1+\delta_{m2})a_k^{nm}\left[\mathcal{L}_{rr}-\frac{2m-3}{\beta_r r}\mathcal{L}_r\right.\\
&\left.+\frac{m(m-2)}{\beta_r^2 r^2}-\frac{m-2}{r}\mathcal{L}_r\left(\frac{1}{\beta}\right)\right]\hat{I}_{n+4-2k}^{m-2}\\
&+(1+\delta_{m1})b_k^{nm}\left[\mathcal{L}_{rz}+\mathcal{L}_{zr}-\frac{2(m-1)}{\beta_r r}\mathcal{L}_z\right.\\
&\left.-\frac{m-1}{r}\mathcal{L}_z\left(\frac{1}{\beta_r}\right)\right]\hat{I}_{n+4-2k}^{m-1}\\
&+\frac{\delta_{m1}}{2}c_k^{nm}\left[\mathcal{L}_{rr}+\frac{1}{\beta_r r}\mathcal{L}_r-\frac{1}{r^2\beta_r^2}+\frac{1}{r}\mathcal{L}_r\left(\frac{1}{\beta_r}\right)\right]\hat{I}_{n+4-2k}^{m}\\
&+d_k^{nm}\left[\mathcal{L}_{rz}+\mathcal{L}_{zr}+\frac{2(m+1)}{\beta_r r}\mathcal{L}_z+\frac{m+1}{r}\mathcal{L}_z\left(\frac{1}{\beta_r}\right)\right]\hat{I}_{n+4-2k}^{m+1}\\
&+e_k^{nm}\left[\mathcal{L}_{rr}+\frac{2m+3}{\beta_r r}\mathcal{L}_r+\frac{m(m+2)}{\beta_r^2 r^2}+\frac{m+2}{r}\mathcal{L}_r\left(\frac{1}{\beta_r}\right)\right]\hat{I}_{n+4-2k}^{m+2}\\
&+c_k^{nm}\left(\mathcal{L}_{rr}+\frac{1}{\beta_r r}\mathcal{L}_r-\frac{m^2}{\beta_r^2 r^2}-2\mathcal{L}_{zz}\right)\hat{I}_{n+4-2k}^{m}\Bigg\}\\
&+\left[\mathcal{L}_{zz}-(1-\omega\delta_{0n})\right]\hat{I}_n^m=-(1-\omega)I_b\delta_{0n}
\end{aligned} \tag{15}$$

Boundary conditions: $(N+1)^2/4$ boundary conditions are required and are derived from the 3-D P_N formulation of Marshak's boundary conditions [13]. The boundary conditions are expressed in terms of local coordinates $\bar{x}$, $\bar{y}$ (tangential to the surface) and $\bar{z}$ (along surface normal $\hat{\mathbf{n}}$), and a rotation function $\bar{\Delta}(-\gamma,-\beta,-\alpha)$ [13] is utilized to rotate local coordinates back to global coordinates for the calculation of boundary conditions, where the α, β and γ are Euler angles [16].

Fig. 2 shows both the arrangements of the global and local coordinates for a general 2-D axisymmetric geometry. β can be calculated from surface normal $\hat{\mathbf{n}}$ as

$$\beta = \cos^{-1}(n_z) \tag{16}$$

The tangential directions of the boundary surfaces are defined in such a way that one tangential direction ($\hat{\mathbf{t}}_x$ or $\bar{x}$) is within the r–z plane and perpendicular to the r-axis, and $\hat{\mathbf{t}}_y$ (or $\bar{y}$) is perpendicular to the r–z plane. Therefore, the Eulerian angle α is related to the azimuthal angle ϕ, Fig. 2(a), as

$$\alpha = \pi + \phi \tag{17}$$

In order to keep $\hat{\mathbf{t}}_y$ (or $\bar{y}$) in the r–ϕ plane, γ=0. With the above conditions, the relationship between the local Cartesian coordinates and the global cylindrical coordinates are

$$\hat{\mathbf{n}} = -\sin\beta\hat{\mathbf{r}} + \cos\beta\hat{\mathbf{z}} \tag{18a}$$

$$\hat{\mathbf{t}}_{\bar{x}} = -\cos\beta\hat{\mathbf{r}} - \sin\beta\hat{\mathbf{z}} \tag{18b}$$

$$\hat{\mathbf{t}}_{\bar{y}} = -\hat{\boldsymbol{\phi}} \tag{18c}$$

from which the derivatives are found to be

$$\frac{\partial}{\partial\bar{z}} = -\sin\beta\frac{\partial}{\partial r} + \cos\beta\frac{\partial}{\partial z} \tag{19a}$$

$$\frac{\partial}{\partial\bar{x}} = -\cos\beta\frac{\partial}{\partial r} - \sin\beta\frac{\partial}{\partial z} \tag{19b}$$

$$\frac{\partial}{\partial\bar{y}} = -\frac{1}{r}\frac{\partial}{\partial\phi} \tag{19c}$$

As an example for the most common case of a fixed-radius cylinder (or wedge), for the vertical wall faces the Eulerian angle $\beta=\pi/2$, and from Eq. (18),

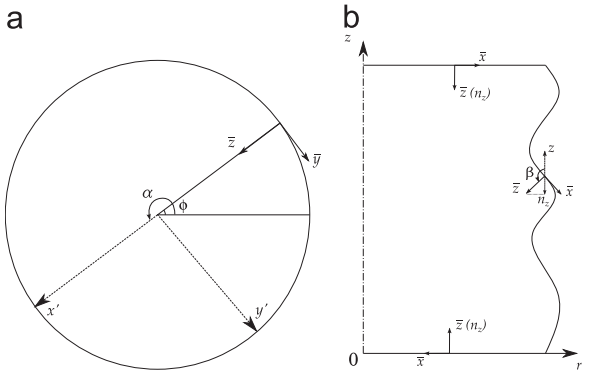

Fig. 2. Schematic of the global coordinate system and the local coordinate system in a general axisymmetric geometry. (a) r–ϕ plane and (b) r–z plane.

$$\hat{\mathbf{n}} = -\hat{\mathbf{r}} \tag{20a}$$

$$\hat{\mathbf{t}}_{\bar{x}} = -\hat{\mathbf{z}} \tag{20b}$$

$$\hat{\mathbf{t}}_{\bar{y}} = -\hat{\boldsymbol{\phi}} \tag{20c}$$

Eq. (18) is also consistent for the bottom and top boundaries of the wedge, where the Eulerian angle β equals 0 and π, respectively.

In order to derive the boundary conditions for the 2-D axisymmetric formulation from the $N(N+1)/2$ boundary conditions of the 3-D formulation [13], the $\bar{\Delta}(-\gamma,-\beta,-\alpha) = \bar{\Delta}(0,-\beta,\pi-\phi)$ in their expanded form [13] are substituted into the full set of Marshak's boundary conditions. In addition, Eqs. (6) and (10) are employed, and the derivatives in the $\bar{y}$–direction are evaluated with Eq. (19c). After tedious derivation, it is found that all $\bar{Y}_n^{-m}$ related boundary conditions become zero identities, which reduces the total number of equations from $N(N+1)/2$ to $(N+1)^2/4$. The $(N+1)^2/4$ remaining boundary conditions are associated with the local spherical harmonics $\bar{Y}_n^m$, for certain combinations of m and n indices, i.e.,

$$m = \begin{cases} 0,1,\ldots,n, & n = 1,3,\ldots,N-2 \\ 0,2,\ldots,n-1, & n = N \end{cases} \tag{21}$$

For example, the boundary conditions for axisymmetric P_3 (where $(N+1)^2/4=4$) are associated with the local spherical harmonics $\bar{Y}_1^0$, $\bar{Y}_3^0$, $\bar{Y}_1^1$ and $\bar{Y}_3^2$.

The complete set of axisymmetric P_N boundary conditions then become

$$\begin{aligned} I_w p_{0,n}^0 = & \sum_{l=0}^{(N-1)/2}\sum_{m'=0}^{2l} p_{2l,n}^m D_{|m||m'|}^{2l}(-\beta)\hat{I}_{2l}^{m'} \\ & -\frac{1}{\beta_r r}\sum_{l=0}^{(N-1)/2}\sum_{m'=0}^{2l}\Big(\delta_m^- u_{li}^m B_{|m-1||m'|}^{2l}(-\beta) \\ & +v_{li}^m B_{|m+1||m'|}^{2l}(-\beta)\Big)\hat{I}_{2l}^{m'} \\ & -\frac{\partial}{\partial\tau_{\bar{x}}}\sum_{l=0}^{(N-1)/2}\sum_{m'=0}^{2l}\Big(\delta_m^+ u_{li}^m D_{|m-1||m'|}^{2l}(-\beta) \\ & -v_{li}^m D_{|m+1||m'|}^{2l}(-\beta)\Big)\hat{I}_{2l}^{m'} \\ & -\frac{\partial}{\partial\tau_{\bar{z}}}\sum_{l=1}^{(N-1)/2}\sum_{m'=0}^{2l} w_{li}^m D_{|m||m'|}^{2l}(-\beta)\hat{I}_{2l}^{m'} \end{aligned} \tag{22}$$

where $i=(n+1)/2$, $\delta_m^{\pm}=(1\pm\delta_{m1})(1-\delta_{m0})$, and the constant coefficients u_{li}^m, v_{li}^m, w_{li}^m, and $p_{2l,n}^m$ are the same as in the 3-D formulation, and the $D_{|m||m'|}^n(\beta)$ and $B_{|m||m'|}^n(\beta)$ are

$$D_{|m||m'|}^n(\beta) = (-1)^{m'} d_{|m|,|m'|}^n(\beta) + d_{|m|,-|m'|}^n(\beta) \tag{23a}$$

$$B_{|m||m'|}^n(\beta) = m'[(-1)^{m'} d_{|m|,|m'|}^n(\beta) - d_{|m|,-|m'|}^n(\beta)] \tag{23b}$$

where the d are Wigner coefficients as given by the 3-D Marshak formulation in [11,13]. The partial derivatives in these boundary conditions are expressed in local optical coordinates as

$$\frac{\partial}{\partial\tau_{\bar{x}}} = \frac{1}{\beta_r}\frac{\partial}{\partial\bar{x}} \tag{24a}$$

$$\frac{\partial}{\partial\tau_{\bar{z}}}=\frac{1}{\beta_r}\frac{\partial}{\partial\bar{z}} \tag{24b}$$

3. Implementation

The solution of the coupled $(N+1)^2/4$ simultaneous PDEs and their boundary conditions is found iteratively by the finite volume based software *OpenFOAM* similar to the *OpenFOAM* implementation of the 3-D P_N [14].

For each Y_n^m PDE, in order to use the Laplacian operator of *OpenFOAM*, the derivatives of $\hat{I}_n^m$ are arranged as

$$\begin{aligned}&\frac{\delta_{m1}}{2}c_2^{nm}\left[\mathcal{L}_{rr}+\frac{1}{\beta_r r}\mathcal{L}_r-\frac{1}{\beta_r^2 r^2}+\frac{1}{r}\mathcal{L}_r\left(\frac{1}{\beta_r}\right)\right]\hat{I}_n^m\\&\quad+c_2^{nm}\left[\mathcal{L}_{rr}+\frac{1}{\beta_r r}\mathcal{L}_r-\frac{m^2}{\beta_r^2 r^2}-2\mathcal{L}_{zz}\right]\hat{I}_n^m\\&\quad+\left[\mathcal{L}_{zz}-(1-\omega\delta_{0n})\right]\hat{I}_n^m\\&\quad=a_{nm}^*\nabla\cdot\left(\frac{1}{\beta_r}\nabla\hat{I}_n^m\right)+b_{nm}^*\hat{I}_n^m+c_{nm}^*\mathcal{L}_{zz}\hat{I}_n^m\end{aligned} \tag{25}$$

where

$$a_{nm}^*=c_2^{nm}\frac{1+\delta_{m1}/2}{\beta_r} \tag{26a}$$

$$b_{nm}^*=c_2^{nm}\left(\frac{\delta_{m1}/2}{r}\mathcal{L}_r\left(\frac{1}{\beta_r}\right)-\frac{m^2+\delta_{m1}/2}{\beta_r^2 r^2}\right)-(1-\omega\delta_{0n}) \tag{26b}$$

$$c_{nm}^*=1-(3+\delta_{m1}/2)c_2^{nm} \tag{26c}$$

All terms other than the $\hat{I}_n^{\pm m}$ are updated before each iteration. The preconditioned conjugate gradient (PCG) [17] algorithm is used to solve each PDE sequentially until $\hat{I}_0^0$ is converged to prescribed criteria.

The boundary conditions expressed in Eq. (22) cannot be directly implemented if the governing equations are solved iteratively. In the *OpenFOAM* implementation of the axisymmetric P_N formulation, the boundary conditions are transformed to Robin-type form to make sure that individual Robin-type boundary conditions can be explicitly associated with each governing equation, i.e.,

$$\hat{I}_n^m+k\frac{\partial\hat{I}_n^m}{\partial\tau_{\bar{z}}}=f\left(\frac{\partial\hat{I}_n^m}{\partial\tau_{\bar{x}}},\frac{\partial\hat{I}_n^m}{\partial\tau_{\bar{y}}},\frac{\partial\hat{I}_{n'}^{m'}}{\partial\tau_{\bar{x}}},\frac{\partial\hat{I}_{n'}^{m'}}{\partial\tau_{\bar{y}}},\frac{\partial\hat{I}_{n'}^{m'}}{\partial\tau_{\bar{z}}}\right) \tag{27}$$

where k is a scalar constant and f is a function of partial derivatives of other intensity coefficients, including the tangential derivatives of $\hat{I}_n^m$.

The boundary conditions are rearranged into matrices and vectors the same way as described in [14]:

$$\mathbf{Q}\cdot\mathbf{I}+\frac{1}{\beta_r}\mathbf{Q}_r\cdot\mathbf{I}+\mathbf{Q}_{\bar{x}}\cdot\frac{\partial\mathbf{I}}{\partial\tau_{\bar{x}}}+\mathbf{Q}_{\bar{z}}\cdot\frac{\partial\mathbf{I}}{\partial\tau_{\bar{z}}}=I_w\mathbf{p} \tag{28}$$

where the $1/\beta_r(\mathbf{Q}_r\cdot\mathbf{I})$ is the second term on the right-hand side of Eq (22). Since $\mathbf{Q}_r$ is a purely geometric quantity, it is better to leave the $1/\beta_r$ outside the matrix. Then in the CFD calculation, just like other matrices in Eq. (28), $\mathbf{Q}_r$ only needs to be calculated once. Eq. (28) can be converted to $N_2=(N+1)^2/4$ Robin-type boundary conditions,

$$\begin{aligned}&(\beta_r+R_{j,j})I_j+Z_{j,J}\frac{\partial I_j}{\partial\bar{z}}\\&\quad=\delta_{j,1}I_w-\sum_{k=1}^{N_2}\left[X_{j,k}\frac{\partial I_k}{\partial\bar{x}}+(1-\delta_{j,k})\left(Z_{j,k}\frac{\partial I_k}{\partial\bar{z}}+R_{j,k}I_k\right)\right]\end{aligned} \tag{29}$$

where $\mathbf{X}$, $\mathbf{Z}$ and $\mathbf{R}$ are defined as

$$\begin{aligned}\mathbf{X}&=\mathbf{Q}^{-1}\cdot\mathbf{Q}_{\bar{x}}\\\mathbf{Z}&=\mathbf{Q}^{-1}\cdot\mathbf{Q}_{\bar{z}}\\\mathbf{R}&=\mathbf{Q}^{-1}\cdot\mathbf{Q}_r\end{aligned} \tag{30}$$

and are evaluated through LU decomposition [18] of $\mathbf{Q}$. A similar stabilizer as in [14] for the 3-D formulation is also defined for the 2-D axisymmetric P_N for optically thin simulations.

4. Results and discussion

Two example problems are presented to explore the accuracy and computational efficiency of the axisymmetric P_N for fields with strongly varying temperatures and absorption coefficients. Although isotropic scattering adds no additional complexity or effort to P_N (as opposite to DOM), all the examples are limited to nonscattering media in this study simply to reduce parameters needed for presentation. In radiative heat transfer problems the "radiative heat source" (or negative divergence of radiative flux) is of greatest interest, which provides the contribution of radiation to the overall energy equation. Physically, the radiative heat source is the difference between local absorption and emission, and the former is quantified by the "incident radiation" G, where

$$-\nabla\cdot\mathbf{q}=-\kappa(4\pi I_b-G),\quad G=\int_{4\pi}I(\hat{s})\,d\Omega=4\pi I_0^0 \tag{31}$$

Wedge enclosure with variable radiative properties: Many combustion problems in a cylinder are axisymmetric,

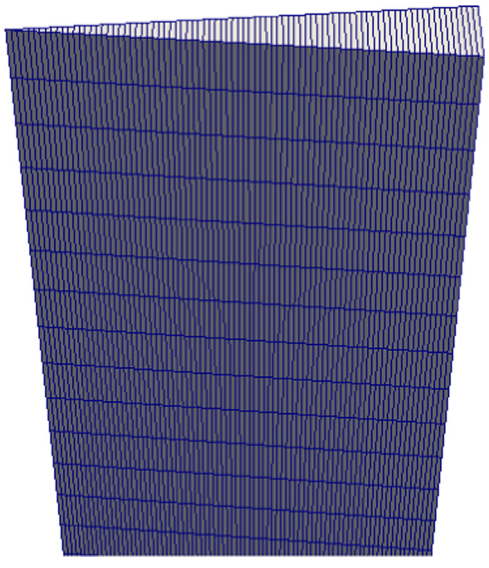

Fig. 3. The mesh of 10° wedge for 2-D axisymmetric P_N testing.

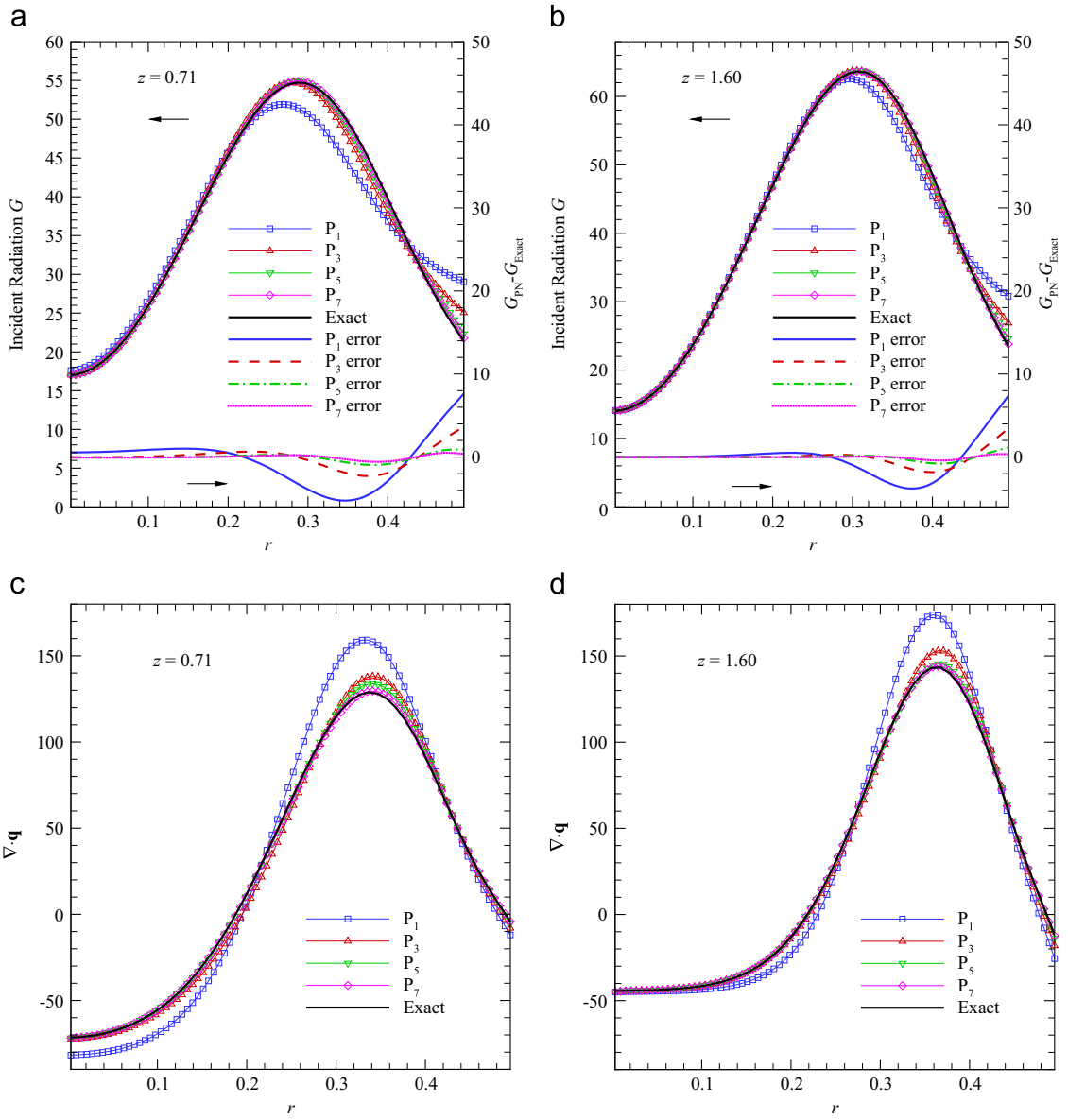

Fig. 4. Incident radiation G and radiative heat source $\nabla \cdot \mathbf{q}$ for a wedge enclosure with variable radiative properties. (a) G at $z=0.71$, (b) G at $z=1.60$, (c) $\nabla \cdot \mathbf{q}$ at $z=0.71$ and (d) $\nabla \cdot \mathbf{q}$ at $z=1.60$.

but CFD codes rarely have cylindrical coordinates and/or axisymmetric capability. In those cases generally a wedge mesh instead of the full cylinder is usually chosen to expedite the computation. The first test case is a wedge with strongly varying absorption coefficient and temperature field as shown in Eq. (32), where κ is the absorption coefficient, and $\beta_r = \kappa$ for non-scattering case. In order to compare with the results from a 3-D cylinder, the mesh shown in Fig. 3 is a 10° piece of the cylinder and the radiative properties are the same as in the cylinder test case [14]. The wedge has 84 cells along the radius and 40 cells along the axis, while the tip of the wedge is cut off to avoid mathematical singularity points. The walls are taken as black cold walls and the center-line is taken as a symmetry plane:

$$I_b = 1 + \frac{20}{R^4} r^2 \left(R^2 - r^2\right) \tag{32a}$$

$$\kappa = C_k \left[1 + \frac{15}{R^4}(R^2 - r^2)^2\right] \tag{32b}$$

$$C_k = 0.3 + z, \quad 0 \le r \le R = 0.5, 0 \le z \le 2.5 \tag{32c}$$

$$\tau_D = 2 \int_0^R \kappa \, dr = 7.5 C_k \tag{32d}$$

The results at two heights are shown in Fig. 4. The results from P_3 to P_7 are very close to the exact solution, while P_1

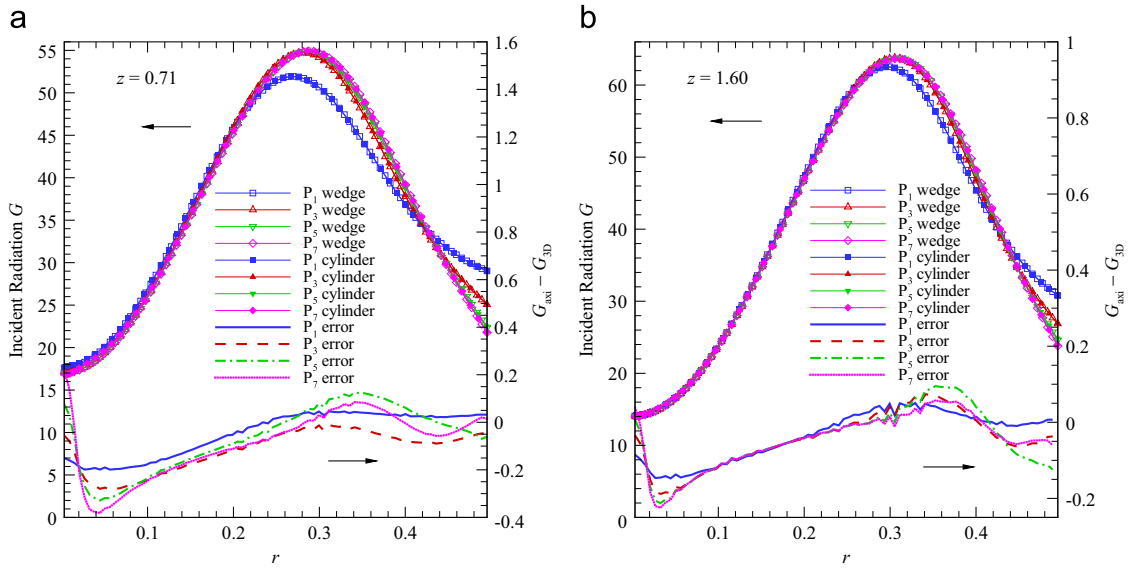

Fig. 5. Comparisons of the numerical results for the 2-D P_N formulation on a wedge mesh and the 3-D P_N formulation on a cylinder mesh. (a) $z=0.71$ and (b) $z=1.60$.

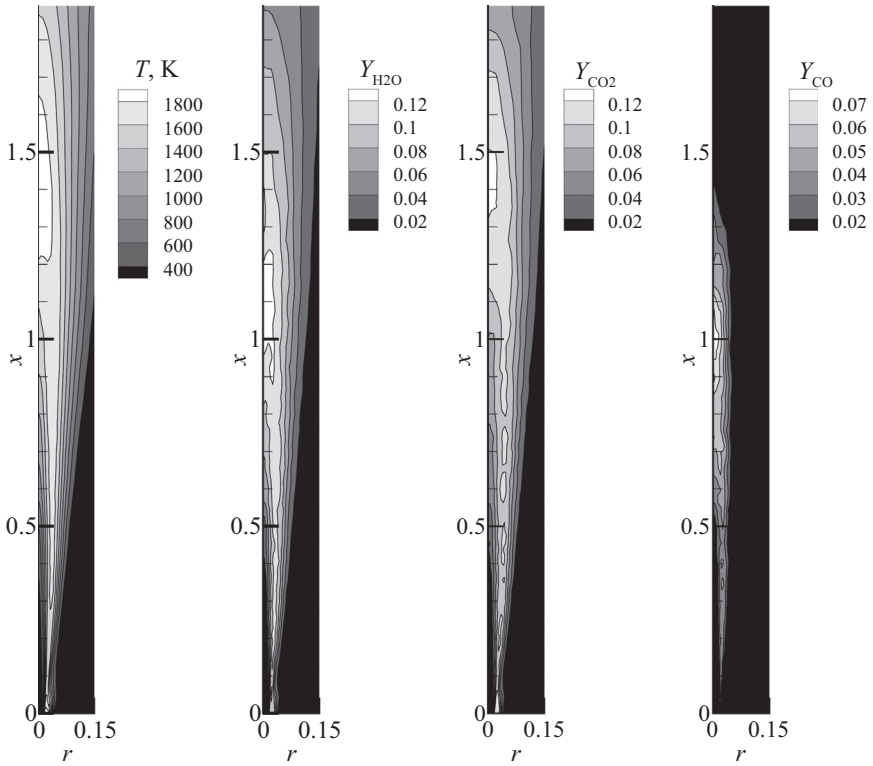

Fig. 6. Mean temperature and mass fraction fields for scaled Sandia Flame D.

has certain levels of discrepancies with the exact solution and the discrepancy decreases with increasing optical thickness. Also the incident radiation G and the radiative heat source $\nabla \cdot \mathbf{q}$ from P_5 and P_7 correctly catch the sharp gradient near the cylinder wall. It is also verified that for this case the axisymmetric P_N results overlap the 3-D results, Fig. 5, to within a maximum discrepancy of 2% close to the center-line of the wedge/cylinder. The difference is due to the square cuboid block mesh at the center of the cylinder and the interpolation between two different

grids. An exact solution for this problem is calculated by direct integration of the RTE [1], which are shown by the black solid lines in the figures.

***Scaled flame with nongray radiative properties*:** The axisymmetric P_N implementation is applied to an axisymmetric methane jet flame. The flame is a four-times scaled Sandia Flame D [19] with temperature and concentration fields strongly varying in both radial and axial directions. The wedge has 84 cells along the radius and 95 cells along the axis, and the walls are taken as black and cold and the center-line is taken as a symmetry plane. Fig. 6 shows the temperature and concentration fields for the quasi-steady flame, which are used as input parameters. The absorption coefficients κ of the participating gases are nongray and are calculated using the *Full Spectrum Correlated-k* (FSCK) model [20,21] requiring a set number of evaluations of the spectral RTE (corresponding to quadrature points in the FSCK scheme). In the present implementation, eight quadrature points are used. The radiative heat source, $-\nabla\cdot\mathbf{q}$, is shown in Fig. 7 for two axial locations. Location $z=1.0$ m is where water vapor has the highest mass fraction, while the maximum mass fraction of carbon dioxide is at $z=1.43$ m. The results calculated by P_1 to P_7 together with the FSCK spectral model on the cylindrical mesh are compared to *line-by-line* (LBL) P_1 calculations and LBL-PMC calculations. The error incurred by FSCK can be evaluated by comparing the FSCK-P_1 results with the LBL-P_1 results, and is essentially negligible for most regions. The LBL-PMC results presented here are calculated on a different streamline-shape wedge mesh [22], and while this is a source of error, major differences between the FSCK-P_N solutions and LBL-PMC results are errors attributable to the P_N methods. As shown in Fig. 7, with the increase of the order of P_N, the results get closer to the LBL-PMC results, and P_5 and P_7 successfully match the PMC results in most regions. The results prove that even under extremely alternating temperature fields and gas concentrations as in real combustion applications, the precision of the FSCK-P_5 and FSCK-P_7 are on the same level as LBL-PMC.

***Computation time comparison*:** A CPU time comparison for different orders of P_N for the above cases is given in Table 1. All calculations were carried out on a single Intel (R) Xeon (R) CPU X7460 running at 2.66 GHz. The P_1 approximation solves a single PDE; P_3, P_5 and P_7 consist of 4, 9 and 16 strongly coupled PDEs with numerous cross-derivatives, respectively. The computation time of the 3-D P_N formulation on the cylinder mesh for both cases is also shown in Table 1. Comparing with the 3-D formulation, the axisymmetric formulation significantly reduces the computing time, which makes P_5 and P_7 competitive for practical applications.

The computation time is strongly related to the number of outer iterations required, which in turn depends on radiative properties. For optically thin cases, a boundary

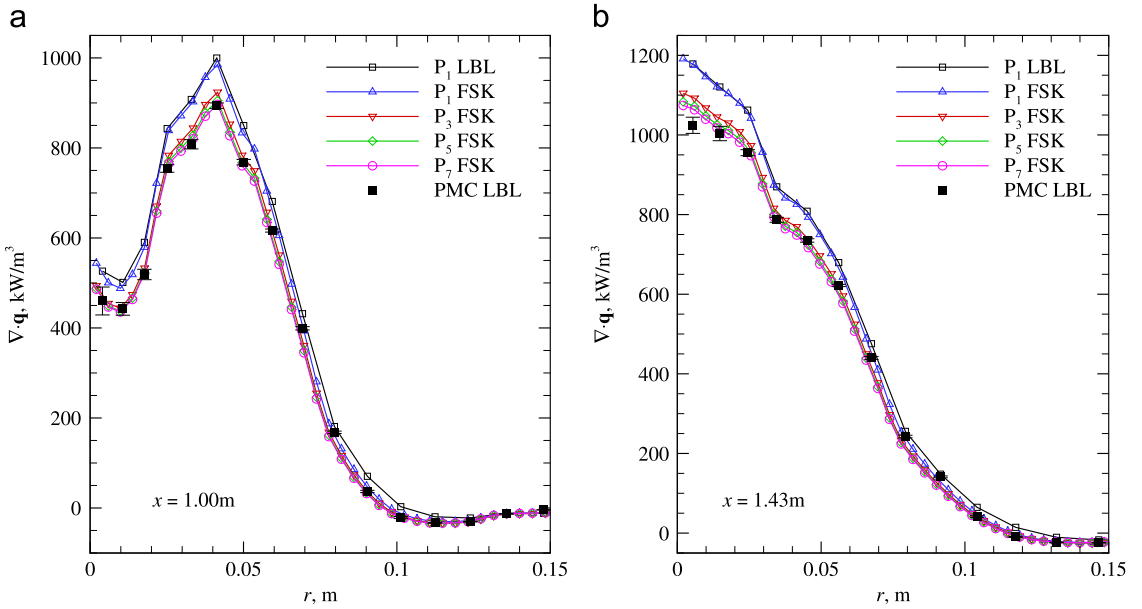

Fig. 7. Radiative source for Sandia FlameD × 4 at two axial locations as calculated with various P_N approximations. (a) $z=1.00$ m and (b) $z=1.43$ m.

Table 1
Comparison of P_N computation cost for different test cases.

Computation cost of P_N method	Number of cells	P_1 (s)	P_3 (s)	P_5 (s)	P_7 (s)
Case I: 3-D Cylinder	131 400	1.01	90.49	269.29	727.08
Case I: 2-D Wedge	3360	0.02	0.57	5.88	11.66
Case II: Flame(3-D, 1 quadrature)	957 600	7.36	1323.53	2566.52	6817.02
Case II: Flame(2-D, 1 quadrature)	7980	0.031	0.73	8.53	14.92

condition stabilizer is utilized for high-order P_N, which will also slow down the convergence.

5. Summary and conclusion

A 2-D axisymmetric version of the spherical harmonics P_N model (up to P_7) is formulated and implemented in *OpenFOAM*. The number of PDEs and intensity coefficients for the P_N-approximation is reduced from $N(N+1)/2$ to $(N+1)^2/4$ by employing axisymmetric relations. The coupled $(N+1)^2/4$ simultaneous PDEs and their boundary conditions are solved iteratively by the PCG method. Two example problems were tested for the 2-D axisymmetric P_N formulation. The new formulation was verified by comparing computations to the intensity coefficients from the 3-D P_N formulation, exact solutions and PMC results. The comparison shows that the 2-D formulation provides an accurate and faster approach for axisymmetric problems. The system of simultaneous PDEs are solved iteratively in the current implementation. Further development could employ a block-coupling approach [23] to improve the stability and computation efficiency.

Acknowledgments

Support by National Science Foundation and the Department of Energy through Grant no. NSF-1258635 is gratefully acknowledged.

References

[1] Modest MF. Radiative heat transfer. 3rd ed. New York: Academic Press; 2013.
[2] Azmy Y, Sartori E. Nuclear computational science: a century in review. Springer; Dordrecht; 2010.
[3] Brunner TA, Holloway JP. Two-dimensional time dependent Riemann solvers for neutron transport. J Comput Phys 2005;210(1):386–99.
[4] Schäfer M, Frank M, Levermore CD. Diffusive corrections to P_N approximations. Multiscale Model Simul 2011:9(1):1–28.
[5] Davison B. Neutron transport theory.London: Oxford University Press; 1958.
[6] Bell GI, Glasstone S. Nuclear reactor theory, vol. 252.New York: Van Nostrand Reinhold; 1970.
[7] Ratzel AC, Howell JR. Two-dimensional radiation in absorbing–emitting–scattering media using the P–N approximation. ASME J Heat Transf 1983;105:333–40.
[8] McClarren RG, Hauck CD. Robust and accurate filtered spherical harmonics expansions for radiative transfer. J Comput Phys 2010;229(16):5597–614.
[9] Mengüç MP, Viskanta R. Radiative transfer in axisymmetric, finite cylindrical enclosures. ASME J Heat Transf 1986;108:271–6.
[10] Ravishankar M, Mazumder S, Kumar A. Finite-volume formulation and solution of the P_3 equations of radiative transfer on unstructured meshes. ASME J Heat Transf 2010;132(2):023402.
[11] Modest MF, Yang J. Elliptic PDE formulation and boundary conditions of the spherical harmonics method of arbitrary order for general three-dimensional geometries. J Quant Spectrosc Radiat Transf 2008;109:1641–66.
[12] Yang J, Modest MF. High-order *P–N* approximation for radiative transfer in arbitrary geometries. J Quant Spectrosc Radiat Transf 2007;104(2):217–27.
[13] Modest MF. Further developments of the elliptic P_N-approximation formulation and its Marshak boundary conditions. Numer Heat Transf—Part B: Fundamentals 2012;62(2–3):181–202.
[14] Ge W, Marquez R, Modest MF, Roy SP. Implementation of high order spherical harmonics methods for radiative heat transfer on OpenFOAM. ASME J Heat Transf 2015;137(5):052701. http://dx.doi.org/10.1115/1.4029546.
[15] Jasak H, Jemcov A, Tukovic Z. OpenFOAM: A C++ library for complex physics simulations. In: International workshop on coupled methods in numerical dynamics, Dubrovnik, Croatia, IUC, 2007. p. 1–20.
[16] Varshalovich DA, Moskalev AN, Khersonskii VK. Quantum theory of angular momentum.Singapore: World Scientific; 1981.
[17] Nocedal J, Wright SJ. Numerical optimization. 2nd ed.Berlin: Springer Verlag; 2006.
[18] Press WH, Teukolsky SA, Vetterling WT, Flannery BP. Numerical recipes—the art of scientific computing. 3rd edCambridge: Cambridge University Press; 2007.
[19] Barlow RS. International workshop on measurement and computation of turbulent nonpremixed flames (TNF), website: ⟨http://www.sandia.gov/TNF/abstract.html⟩.
[20] Modest MF. Narrow-band and full-spectrum *k*-distributions for radiative heat transfer—correlated-*k* vs. scaling approximation. J Quant Spectrosc Radiat Transf 2003;76(1):69–83.
[21] Modest MF, Riazzi RJ. Assembly of full-spectrum k-distributions from a narrow-band database; effects of mixing gases, gases and nongray absorbing particles, and mixtures with nongray scatterers in nongray enclosures. J Quant Spectrosc Radiat Transf 2005;90(2):169–89.
[22] Wang A, Modest MF. Spectral Monte Carlo models for nongray radiation analyses in inhomogeneous participating media. Int J Heat Mass Transf 2007;50:3877–89.
[23] Ferziger JH, Perić M. Computational methods for fluid dynamics. 3rd edBerlin, Heidelberg: Springer; 2001.